

Hydro-power structure affected by alkali-aggregate reaction: a case-study involving numerical re-assessment

*J.-F. Seignol¹⁾, L.-I. Boldea²⁾, R. Leroy³⁾,
B. Godart⁴⁾, J.-G. Hammerschlag⁵⁾

- 1) *Structures monitoring and pathologies service, LRPC Clermont-Ferrand, France*
 - 2) *Stucky, Lausanne, Switzerland*
 - 3) *ALPIQ, Lausanne, Switzerland*
 - 4) *LCPC, Bridges Department, Paris, France*
 - 5) *Holcim (Suisse) SA, Product Management, Eclépens, Switzerland*
- 1) *jean-francois.seignol@developpement-durable.gouv.fr*

ABSTRACT

This communication describes a case-study concerning a real hydraulic power-plant affected by AAR. The displacements imposed to the sensitive equipments (pumps, turbines, pipes...) are difficult to predict due to the complexity of the structure and strongly heterogeneous moisture distribution. Hence the prediction of serviceability and the managing of the plant require the complete chemo-mechanical modeling of the structure.

Using a worked out constitutive model designed to take into account influence of moisture and temperature on both kinetics and amplitude of AAR, the different phases aiming to the re-assessment of the structure are presented: monitoring of the structure, data collection from material samples, fitting of the numerical model, validation and exploitation. The paper focuses on the fitting of the model based on global and local strain monitoring. It aims to demonstrate the efficiency of a global method based on both field monitoring and numerical re-assessment to answer a critical structure-management problem.

1 INTRODUCTION

Hydro-power facilities represent a significant part of Alkali-Aggregate Reaction (AAR) affected concrete structures (Charlwood and Sans 2007) and deserve particular attention. They indeed involve very large concrete volumes in which water (a mandatory AAR co-factor) is abundant. Their serviceability might be strongly disturbed by concrete strains, due to several equipments (valves, turbines, generator, pipes...) set in the structure. Moreover, stopping these facilities (for repair or because of serviceability loss) often involves high costs, economically and socially speaking.

When a pathology such as AAR is diagnosed in a dam or in a powerplant, the ability of re-assessing it, especially its stress-state which influences its reliability, becomes crucial, as is the precise prediction of both amplitude and rate of future displacements imposed to the equipments by the concrete swelling. For the structure manager, it is a *sine qua non* condition to choose a strategy: adaptation of equipments, repair of the structure...

The present paper intends to present an in-progress case-study concerning a real hydro-power plant. This facility behaviour is complex, difficult to evaluate without the use of detailed numerical model. Its response to AAR is difficult to assess due to highly heterogeneous moisture field and highly redundant structure. To precisely answer structure owner concerns about stress-state and disturbing displacements of equipments anchorage points, a study was started a few years ago. It involves structure monitoring, large material sampling for laboratory tests and the use of a chemo-mechanics numerical model to re-assess the behaviour of the plant.

The first part of the paper describes the AAR-affected power-plant and the goals of the study from the structure-owner point-of-view. Then monitoring systems and material tests are presented. The third part focuses on the numerical models used for the predictive evaluation, detailing the four-step procedure: mesh, numerical evaluation of moisture, fitting of expansion model based on material tests, and chemo-mechanical modeling of the structure. The fourth part of the paper discusses numerical results and compares them to field monitoring.

2 THE POWER-PLANT AND ITS PATHOLOGY

2.1 Veytaux power-plant



Figure 1: Hongrin dams (north 125 m / south 95 m high)

In December 2008, Énergie de l'Ouest-Suisse and Atel have merged to create Alpiq, the new Swiss energy market leader with a strong European orientation. In its role of hydro-power asset manager, Alpiq is in charge of the company "Forces Motrices Hongrin-Léman

(FMHL)". FMHL was founded in 1963 to set up a hydro-power development including pumped storage. Since 1970, when the plant was put into service, EOS (now Alpiq) has been responsible for its operation. This is the reason why orders such as start/shutdown or production/pumping regulation are remote controlled from the Alpiq-Swissenergy headquarters in Lausanne. With its large flexibility, the 4 x 60 MW pumping-generation (see Figure 2) Veytaux power plant is very important for the transmission network to ensure as high a degree of secure supply in west part of Switzerland.



Figure 2: Machine room in Veytaux plant (4 groups of pump/turbine)

The reservoir collects the water of natural contribution, rainfall and melted snow, as well as the water pumped from Lake Geneva. It has a capacity of 52 million m³. The dam, built at an altitude of 1'255 m, is composed of two arches across the Hongrin and Petit-Hongrin rivers. The pumps of the Veytaux underground plant are driven by low cost electricity from the grid, mainly at hours of low consumption. These pumps force back water from Lake Geneva (24 m³/s) into the Hongrin reservoir, some 800 m higher up. This water is then turbined in the Veytaux plant by four generating sets, to produce up to 240 MW of power at hours of peak consumption. In order to bring back one m³ of water up into the Hongrin reservoir, 2.7 kWh of night power is needed. This same m³ produces approximately 2 kWh during peak hours. This pumped storage cycle transfers an amount of electricity from night to day, from hours of cheap and not used electricity to hours of high consumption.

The plant consists of four quite similar blocks, side by side in a rock pit. Each block is about 30 m by 30 m and its three stories represent about 10 m high. Each block is composed of an upper slab (level 0) on which hydro-power equipments (pumps, turbines, pipes...) are anchored. Upper slab is supported by various walls delimiting technical spaces

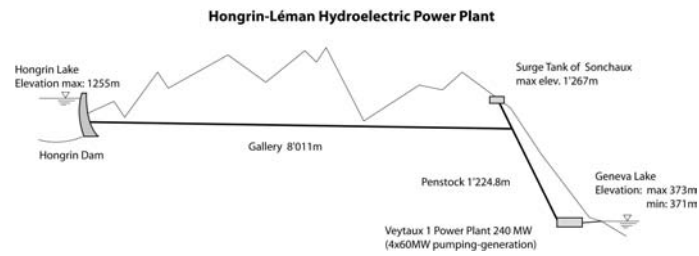


Figure 3: Hongrin-Léman Hydroelectric Power Plant

in levels -1 and -2. Along one of the sides is the outlet channel, allowing water to reach Lake Geneva after activating the turbines. This channel represents the main moisture source in the concrete structure. Figure 4 presents a cross-section of the plant.

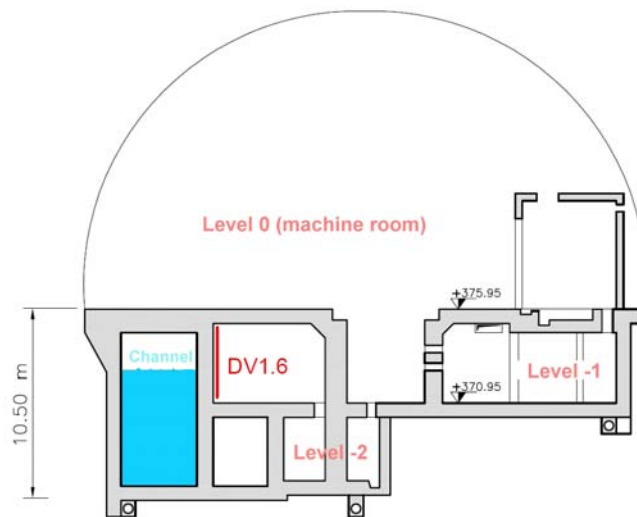


Figure 4: Vertical cross-section of the plant with the location of Deflectometer DV 1.6

2.2 AAR in the power house

Since the commissioning of Veytaux power house in 1972, movements in the slab at the level of the machine room were observed, as well as mechanical problems during the review of the valves, turbines and pumps. These repetitive problems tend to increase during each revision and corrective measures, such as grinding the bolt holes are no longer sufficient to compensate the movements.

The laboratory tests conducted on cores taken from the concrete of the plant have confirmed the presence of alkali-aggregate pathology. The results obtained are insufficient to permit assessment of the current strength of the structure and a prediction of its future behaviour.

To improve the understanding of the phenomenon and define more precisely the future

evolution of expansion, a complete modeling of the structure behaviour has been performed. This model required incorporating, in addition to the concrete characteristics, the knowledge of the strains, thermal and hydraulic conditions in function of time. These parameters are essential to evaluate the progress of the concrete expansion.

2.3 Goals of the case-study

The first goal of this study is to assess the structural safety of the plant, for both present and future times. Two kinds of questions shall be answered:

- Is the structure stress state, resulting from both service loads and restrained chemical swelling, consistent with material strength?
- What are the forces in the equipments (in particular in the pipes bringing the high-pressure water to the turbines) due to anchorage points movements generated by slab deformation?

The structure management also requires informations to assess future serviceability of the facility. Concrete strains already involve regularly setting equipments (especially lining up pumps, turbines and alternators axis) and the future deflections have to be predicted to decide whether equipments backlash will be sufficient.

3 FIELD MEASUREMENTS AND LAB TESTS

3.1 Measurement concept

The more precise the measurements are performed, the more it is possible to identify the alkali-reaction phenomenon and its relationship with external parameters such as relative humidity and air temperature, or when water is present or not in the rock or in the channel.

The measurement system consists of four types of data needed for understanding the behaviour of the power house structure. The different types of measurements made are summarized in table 1.

The plant has four generating units (pump-turbine) on four identical separate blocks. To avoid too many monitoring instruments but nevertheless allow a statement as detailed as possible for all components of a block, only the block No. 1 was equipped with measuring devices.

In total, 18 “Deflectometers” (strain measurements with invar wire), 36 thermometers and 32 probes for relative humidity of concrete and air were finally installed.

As variations of air temperatures can change rapidly depending on the use or not of the units, and in order to analyze in detail the effects of these variations on the structure, the readings were made every hour.

As strains due to the alkali-reaction were very small compared to the thermal movements, the measurements had to be carried out over a period of two years before getting clear results. But they continue (and will continue for a few years still) to confirm the initial results.

Table 1: Different devices for structure monitoring

Type of measurement	Requirements	Remarks
Absolute displacement	Accuracy: 0.10 mm; Amplitude: 5 mm	Conventional surveys of point at Level 0, on which will be based the relative deformations.
Relative strains	Accuracy: 5 $\mu\text{m}/\text{m}$; Amplitude 0.5%	Invar wire measurements on the surface of walls and slabs.
Temperature	Accuracy: 0.5 $^{\circ}\text{C}$; Amplitude 0 to 50 $^{\circ}\text{C}$	Measurements of air, water and concrete (walls, slabs, invert).
Relative humidity	Accuracy $\pm 2\%$; Amplitude: 0 to 100%	Measurements of air, water and concrete (walls, slabs, invert).

3.2 Details and results of strain measurements

Among the main elements of the structure, the bearing walls at levels -1 and -2 and the slab level of the machine room are of particular interest as they participate actively in the emergence of the movements observed. It is therefore mainly on those items that all the monitoring equipment was placed. The locations of all the deflectometers are shown in Figure 5. In this figure, probes for measuring temperature and relative humidity are also represented. Their results are presented in the next subsection.

The strain measurement equipment with an invar wire of a diameter of 0.12 mm was chosen for the following reasons:

- Good accuracy ($< 5 \mu\text{m}/\text{m}$);
- Ease of implementation and recording of measurements;
- Limited costs;
- Possible further relocation of the sensors for measurements in other places inside the plant or in other works.

The system consists of a fixed anchor on one side of the wire and, at the other end, a sensor and a counterweight to keep the wire with a constant tension. The lengths of the wires were chosen according on the available place in each measuring location and lengths are from 3 to 16 meters.

The measurements were influenced by the plant vibrations and the rapid air thermal variations due to the starting and stopping of the units (up to 5 $^{\circ}\text{C}$ over 24 hours). The final calculation of deformations had to take into account these thermal effects and find average values to soften the vibration effects.

Finally, the observed strains are very small for the horizontal movements but the average of the vertical wires is showing an increase of about 15 μm per meter and per year. The maxima were found with more than 35 $\mu\text{m}/\text{m}/\text{year}$, for the walls in contact with the water channel. This last value represents a concrete expansion of 3.5 mm every 10 years over a wall height of approximately 10 meters.

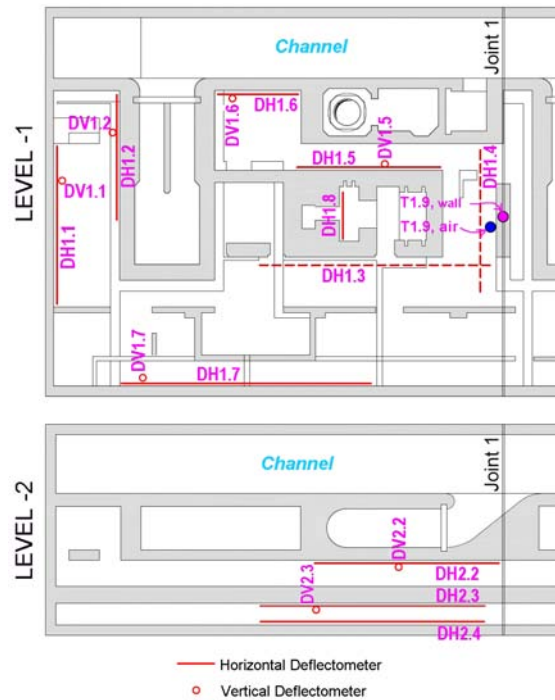


Figure 5: Location of strain measurements and probes in the plant

Figure 6 shows the strains measured with the vertical invar wire at level -2 from 2006 to 2008. It shows the concrete strains due to the effect of temperature variations (amplitude of about 0.3 mm) and the visible “noise” along the mean curve is due to combined effect on the invar wire of the ambient air temperature variations and vibrations of the plant.

3.3 Details and results of temperature and humidity measurements

The choice of independent dataloggers was done to facilitate the installation of instruments and allow a good flexibility to relocate them to different parts of the plant if needed.

Each datalogger can record up to 4 sensors and store several months of data. On most dataloggers two probes were connected, each one equipped with a relative humidity sensor and a thermometer.

The 18 dataloggers worked all perfectly. Only a few humidity sensors have been destroyed by direct contact with water (arrival of water through the concrete or drops of condensation). Inside the concrete, the probes were placed in holes of 15 cm deep.

The graph in Figure 7 represents the variations of temperatures in and around the concrete wall of an intermediate wall (no contact with water or rock). The large temperature variations observed by the ambient air sensor can be seen, as well as the strong influence of units operating or not (the stopping of group 1 for maintenance work in 2006-2007 is clearly visible). Temperature recorded inside the concrete is much more stable with changes being attenuated by the concrete mass.

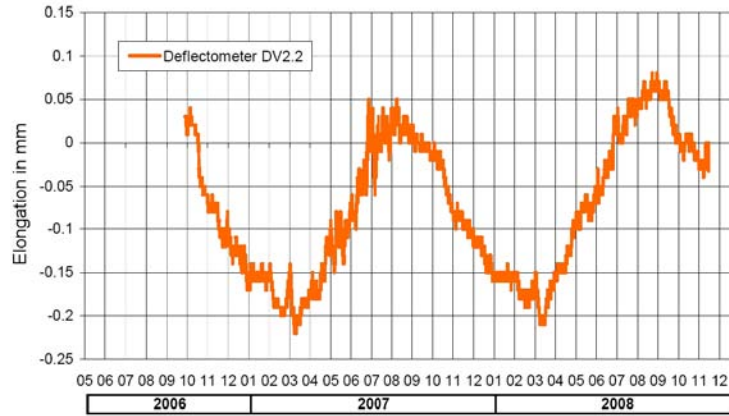


Figure 6: Strains measured by Deflectometer DV2.2 (invar wire)

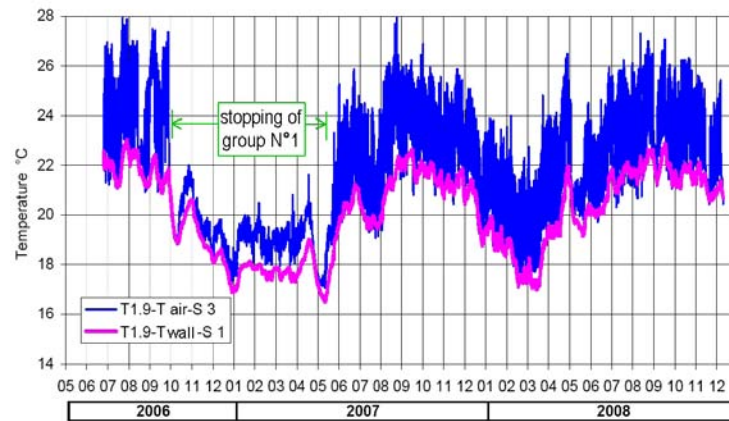


Figure 7: Temperature monitored around and inside an intermediate concrete wall

Figure 8 represents the relative humidity recorded on the same intermediate wall. Globally, the measurements showed that relative humidity found in the walls which are not in contact with water or rocks around the cave varies between 70 and 85%. Those walls in contact with water are showing a relative humidity of 90% or more.

3.4 Absolute movements

For 23 years surveying is also performed on many points within the plant. These deformation survey points are located at different locations on the slab of level 0 of the machine room (blocks 1 to 4) and on certain elements of pump and turbine. The results of these measurements help to define the absolute movements of the entire plant.

These measurements are presented and exploited in subsection 4.6.

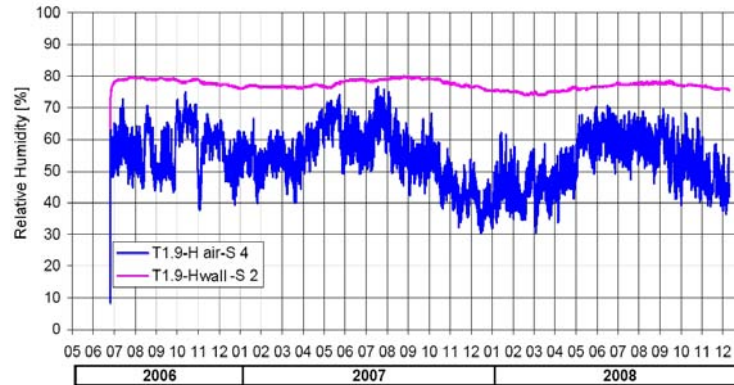


Figure 8: Relative humidity monitored around and inside an intermediate concrete wall

3.5 Calculation of irreversible strains

As mentioned earlier, the largest strains were measured on the vertical walls and more specifically on the walls in direct contact with water. As the influence of temperature was very important on the concrete strains and partly on the invar wire, the final irreversible strains were obtained by selecting times of equal thermal conditions and then to compare the two measured strain values.

The graph in Figure 9 shows the calculation made on a vertical wire (length 3.80 m) set in the channel wall (Deflectometer DV1.6, the location of which can be seen in Figure 4). On this graph are shown two lines giving the two calculated trends of irreversible concrete strain. The expansion trends computed in this example are around $+ 37 \mu\text{m}/\text{m}/\text{year}$.

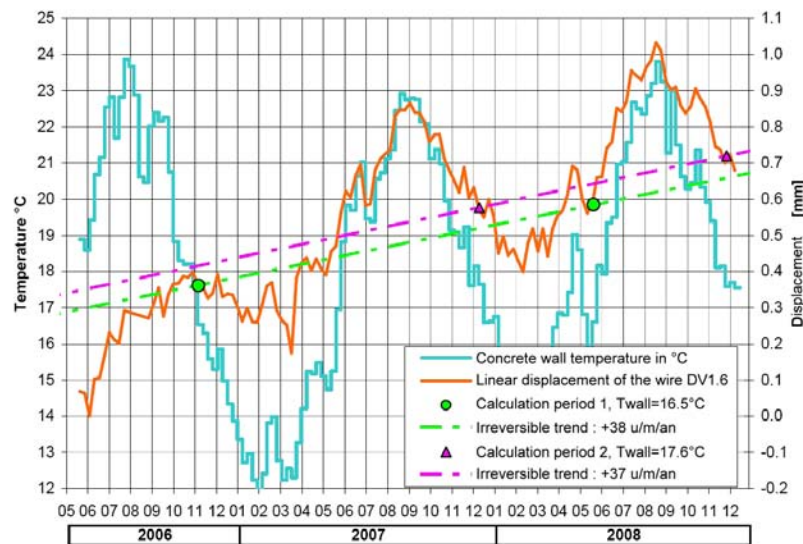


Figure 9: Calculation of irreversible concrete strains based on wire DV1.6 measurements

3.6 Material tests

Several samples were also taken from the concrete structure in order to evaluate physical, chemical and mechanical properties of the material. 13 locations were considered as representative of the whole plant (2 in the upper slab of machine room, 4 in the walls and 1 in the slab for level -1 and 5 in the walls and 1 in the slab for level -2). At each one, several sample cores were drilled out and used for different laboratory tests (Young modulus, density, compressive and tensile strengths, water and air permeability, thermal conductivity, coefficient of thermal expansion, alkali-content...)

Moreover, for each location, three cylindrical sample cores were used for accelerated residual expansion tests (Fasseu 1997).

4 NUMERICAL MODELING

The numerical modeling of block 1 is realized with ALKA module from Finite-element-method software CESAR-LCPC (Humbert et al. 2005). This module deals with mechanical consequences of AAR development in concrete structures (Li and Coussy 2002a). To take into account concrete thermo-hydraulic state on both AAR kinetics and amplitude (Larive et al. 2000; Ulm et al. 2000), it considers temperature and moisture fields in the structure as input data. These fields are computed with DTNL module in CESAR-LCPC, devoted to transient non linear diffusion problems. The main advantage in this method is the use of the same FEM-mesh for the three computations.

Each computation is ran with constant time-steps equal to 1 year. Let $t_0 = 0$ denote initial time corresponding to the end of plant construction (year 1968), $t_p = 40$ years present time and t_f final time corresponding to a 100-year design service-life. The different problems (hydraulic, thermal and chemo-mechanical) are solved for times $(t_i)_{i=1\dots n}$ with $n = 40$ (modeling of present state) or $n = 100$ (predictive modeling).

4.1 Geometrical model

Block 1 is represented by a mesh composed of 20,532 solid elements with quadratic interpolation, as shown on Figure 10. It contains 93,636 nodes. The spatial discretization pace was chosen in order to count sufficient number of nodes in each wall thickness to correctly represent strong moisture gradients between immersed and aerial zones. The whole geometrical model is relatively complex in order to take into account the various contribution of each structural elements to the upper slab displacements.

4.2 Thermal and hydraulic problems

Both thermal and hydraulic problems consist in solving the PDE

$$\frac{\partial Q}{\partial t} - D \frac{\partial^2 Q}{\partial x^2} = 0, \quad (1)$$

where Q represents unknown field (temperature T or relative humidity h) and D the material diffusivity, based on laboratory tests realized on concrete sample cores. For the thermal problem, $D = 6.10^{-2} \text{ m}^2.\text{day}^{-1}$; for the hydraulic one, $D = 5.55 \cdot 10^{-4} \text{ m}^2.\text{day}^{-1}$.

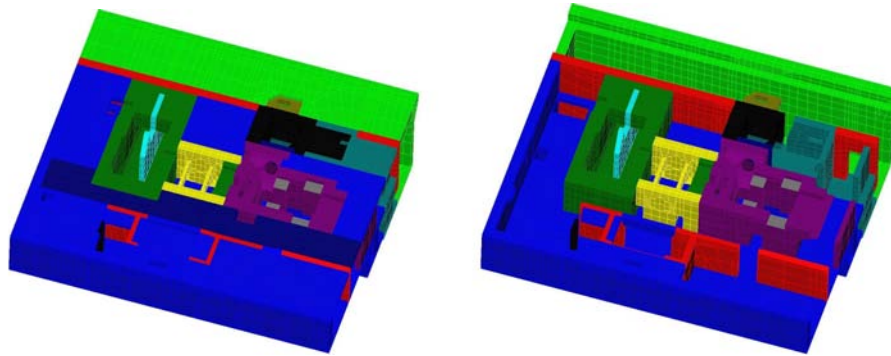


Figure 10: FEM-mesh representing block 1 of the plant, with and without upper slab (outlet channel is in light green, dark green is for turbine pit, purple one for the pump)

Thermal computation is ran with prescribed temperatures as boundary conditions. These temperatures are obtained from structure monitoring. Due to the large time-step by comparison to characteristic time for thermal conduction, the thermal problem is solved as a steady-state problem.

For hydraulic problems, five types of boundary conditions are considered:

- Walls in contact with water (such as channel walls) are submitted to prescribed h of 100%.
- External faces of the structure, in contact with saturated rocks are also submitted to prescribed h of 100%.
- Walls in contact with air have a prescribed h equal to the one measured by the different moisture probes.
- Element faces on the border between blocks 1 and 2 belong to a plane of symmetry for the moisture diffusion problem, hence the moisture gradient is equal to 0.
- Inner faces of turbine pit are watertight by metal plates, stopping the moisture flow; once again, moisture gradient will be null.

The modeling starts with an uniform initial value of 80%.

Figure 11 exhibits some moisture contour-plots at t_p . One shall notice the strong moisture gradients in the walls between immersed and aerial zones.

4.3 Chemo-elastic constitutive equation

Constitutive model used to simulate AAR influence on concrete structure was developed by (Li et al. 2000; Li et al. 2001; Li and Coussy 2002a). Its main features are briefly presented here; reader should refer to literature for further details. Based on a mesoscopic material description, the model represents AAR development as the expansion of gel in concrete porous network, considered as elastic. Gel swelling is supposed to be in linear relation with chemical extent ξ and it induces a pressure $k.\xi(t)$ on solid skeleton. With some simple

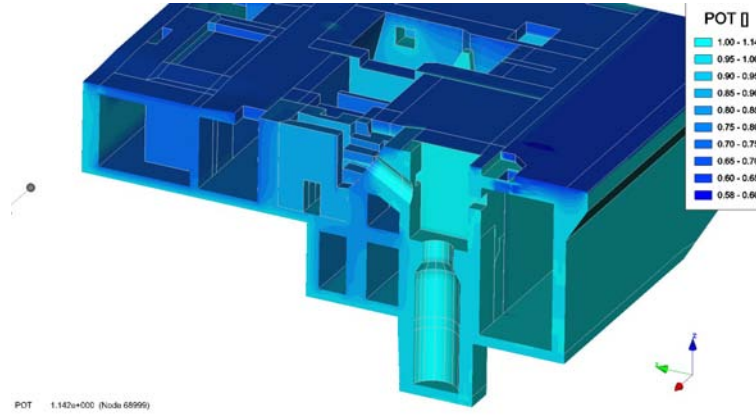


Figure 11: Contour-plot for relative humidity in a cross section of the plant (light blue represents high moisture)

assumptions (Li et al. 2000), the 1-dimensionnal constitutive equation of AAR-affected concrete can be written as an additive relation:

$$\varepsilon = \varepsilon_e + \varepsilon_\infty \cdot \xi(t), \quad (2)$$

where ε_e represents the elastic part of the strain and ε_∞ is the maximal strain observed on stress-free concrete. The evolution of ξ with time t is given by Larive law:

$$\xi(t) = \frac{1 - \exp(-t/\tau_c)}{1 + \exp\left(\frac{\tau_l - t}{\tau_c}\right)}, \quad (3)$$

τ_c being AAR-characteristic time and τ_l its latency time.

Thermo-hydral state (T, h) influences AAR through coupling laws (Ulm et al. 2000; Seignol et al. 2006) between T , h and parameters ε_∞ , τ_c and τ_l . As shown by several experimental studies, there is no coupling between T and ε_∞ .

4.4 Expansion model fitting

In order to assess values for parameters ε_∞ , τ_c et τ_l needed by model (2), (3), free expansion tests should be used. The problem stands in the fact that the sample cores drilled out of the structure have already started to swell in uncontrolled conditions, different from normalized ones described in test protocol (Fasseu 1997). When they are put in the reactor, with constant temperature T_0 of 38 °C and relative humidity $h_0 = 100\%$, they already have a chemical-strain of unknown value ε_i . Let t_i be the unknown time during which the sample should have been put into the reactor to reach this expansion ε_i .

Ergo, when the residual expansion test is performed, the monitored strain is not the global free expansion history $\varepsilon_\chi(t)$ for $t = 0$ to $t = \infty$, but a strain-increment $\Delta\varepsilon_\chi(t - t_i) = \varepsilon_\chi(t) - \varepsilon_i(t_i)$.

Fitting chemical swelling model is a two-phase process, based on an inverse problem approach (Li and Coussy 2002b; Li and Capra 2004). First, the parameters for equations

(2), (3) are fitted by taking arbitrary (but realistic) values for ε_i and t_i . Let $(\varepsilon_i^{(k)}; t_i^{(k)})$ be such an assumption. The three parameters $(\varepsilon_\infty^{(k)}; \tau_c^{(k)}; \tau_l^{(k)})$ can then be assessed by using experimental values from a residual expansion test, as shown on Figure 12.

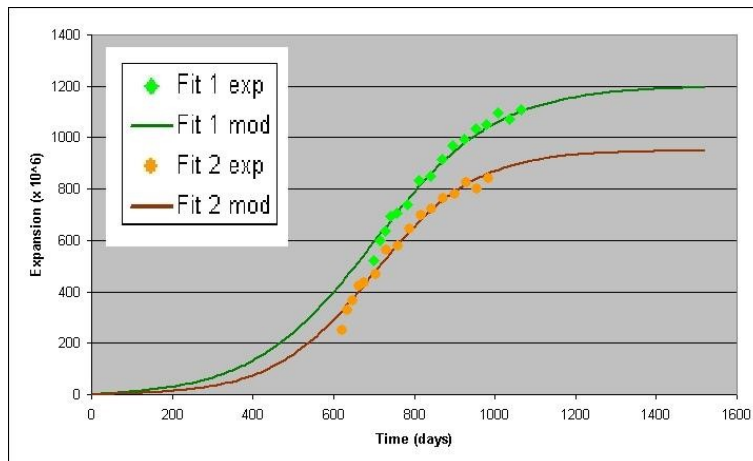


Figure 12: Fitting of Larive model on experimental data, based on two different initial parameters sets (1 is for $t_0 = 700$ and $\varepsilon_0 = 520$ and leads to $\varepsilon_\infty = 1200$ and $\tau_c = 150$; 2 is for $t_0 = 620$ and $\varepsilon_0 = 250$ and leads to $\varepsilon_\infty = 950$ and $\tau_c = 125$)

This process is repeated with different assumptions (here, $k = 1 \dots 9$). In each case, a complete modeling of the structure is realized, and the obtained results are compared to data from in-situ monitoring. The model is then fitted with the parameter set which gives the least discrepancy.

In the case of Veytaux power-plant, residual expansion test for location R6 was used, since this zone exhibited the largest residual expansion, therefore the largest data set. Comparison between different computations and monitoring is based on the absolute vertical displacement of five surveying points, as described in subsection 4.6.

4.5 Chemo-elastic computation

First, a chemo-elastic modeling is realized without any mechanical loading (no dead weight, no forces due to equipments...). In this way, obtained strains and displacement are only due to AAR effects and can be directly compared to in-situ monitoring (otherwise, the computed strains would result from both chemical and mechanical effects, since monitoring of the structure is realized by considering the loaded plant as a reference). Note that this decomposition of the problem is possible since our model does not take stress influence on AAR into account (this point should be soon introduced in the model, based on experimental results by (Multon and Toutlemonde 2006)).

Boundary conditions consist in prescribed displacement: every face in contact with surrounding rock or on the plane of symmetry between blocks 1 and 2 is given a normal displacement equal to 0.

Outside swelling parameters, presented in the next subsection, concrete constitutive

equation needs a linear elastic part. Based on laboratory tests realized on sample cores, Young modulus $E_c = 30$ GPa and Poisson ratio $\nu = 0.2$ are chosen

4.6 Expansion law determination

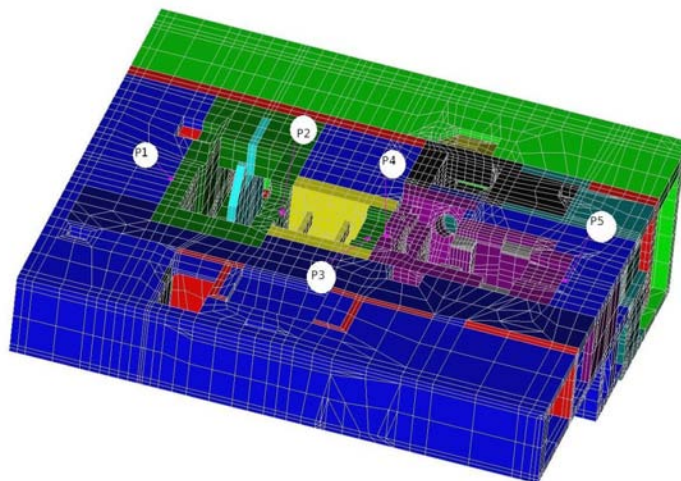


Figure 13: Position of the different surveying points used to fit the swelling law

Computations were realized with nine different parameter sets for chemical model (2)-(3). Each computation result is compared to field measurement of vertical displacement realized since time $t_s = 17$ (corresponding to year 1985) for surveying points. For every point $(P_i)_{i=1\dots 5}$, presented in figure 13, vertical displacement history $w_{mon,i}(t)$ for $t_s \leq t \leq t_p$ is known, as well as nine series of displacements $w_i^{(k)}(t_j)$, $k = 1\dots 9$ and $j = 17\dots 40$ computed with different expansion laws. But the surveying points had already started to move before t_s , without being monitored. Hence, for each computation to check, the in-situ displacements will be shifted by a value obtained from numerical modeling at time t_s . Numerical results will be compared to reference displacement histories

$$w_{ref,i}^{(k)}(t_j) = w_i^{(k)}(t_s) + w_{ref,i}(t_j). \quad (4)$$

The discrepancy of computation (k) is given (in mm) by

$$e^{(k)} = \frac{1}{5} \sum_{i=1}^5 \sqrt{\frac{1}{23} \sum_{j=17}^{40} \left(w_i^{(k)}(t_j) - w_{ref,i}^{(k)}(t_j) \right)^2}. \quad (5)$$

Figure 14 presents some comparisons between three computations for surveying point P_1 .

A preliminary parametric study, not presented here due to lack of space, led to an estimation for τ_l of 700 days. It was aimed to narrow the number of parameter sets to test. Table 2 presents different expansion laws tested, as well as the corresponding discrepancy.

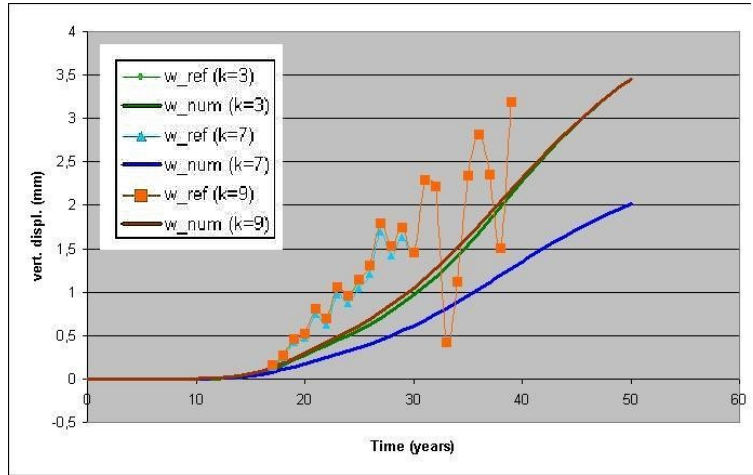


Figure 14: Vertical displacement versus time at point P1 for three different parameter sets

Table 2: Parameters sets and estimated error for each computation

k	ε_{∞} ($\mu\text{strains}$)	τ_c (days)	$e^{(k)}$ (mm)
1	700	100	0.764
2	950	100	0.684
3	1200	100	0.612
4	700	125	0.755
5	950	125	0.612
6	1200	125	0.599
7	700	150	0.745
8	950	150	0.660
9	1200	150	0.586

The best set is given by case number 9, which is:

$$\begin{cases} \varepsilon_{\infty} = 1200 \cdot 10^{-6}, \\ \tau_c = 150 \text{ days}, \\ \tau_l = 700 \text{ days}. \end{cases}$$

Figure 15 shows the fair agreement between the fitted model and the monitoring of surveying points. The general tendency is correctly reproduced even if the model does not represent the cyclic variations of these displacements (as mentioned above, the power-plant is very sensitive to temperature variations induced by different operating phases). The model might be slightly under-estimating the largest displacements, but this discrepancy is about 1 mm, which lies in the acceptable error range of the modeling.

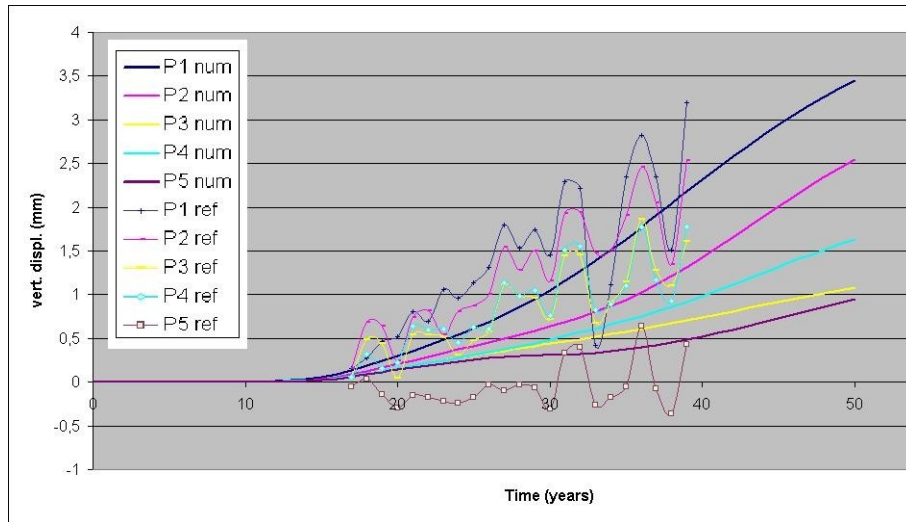


Figure 15: Vertical displacement versus time for different surveying points

5 DISCUSSION

Figure 16 presents structure deformation induced by AAR development until time t_p (at the age of 40-year old), then a predicted deformation for $t_f = 100$ years. This explains how the reaction is moving the upper slab in three directions, which brings about a problem for operating hydro-power equipments. The strong influence of heterogeneous moisture field is exhibited with predominant expansions above the outlet channel, as well as the role of the walls, with different thicknesses, generating various “peaks” in the raise of the slab.

5.1 Modeling validation

The modeling presented above is then compared to other field monitoring in the plant. Two types of results can be used to evaluate this simulation. First, some sample cores drilled from the most damaged parts of the structure (locations R3, R5 and R8) did not exhibit residual expansion in laboratory reactor: all the reactive silica or alkaline was already consumed at the time of drilling. If the modeling is correct, the computed chemical extent ξ in these zones should reach the limit value $\xi = 100\%$ for drilling time t_p . The computation gives extent equal to 84%, 100% and 40%, respectively. The two first locations are validated, whereas the last one will deserve deeper inquiry.

The second validation test for the modeling consists in comparing numerical data to strain rates measured by some horizontal and vertical distancemeter set on the structure walls. Here, results for distancemeters DH 1.2 and DV 1.2 (wall of the turbine pit in level -1) and DH 1.6 and DV 1.6 (wall between the outlet channel and technical space in level -1) are used, since they gave the largest strain-rates. For each of them, Figure 17 presents computed strains versus time and a stroke corresponding to the measured strain-rate. It can be seen in this figure that monitored strain-rates give values very close to the tangent of the different strain curves. These values are presented in table 3. The precision of distancemeters (about

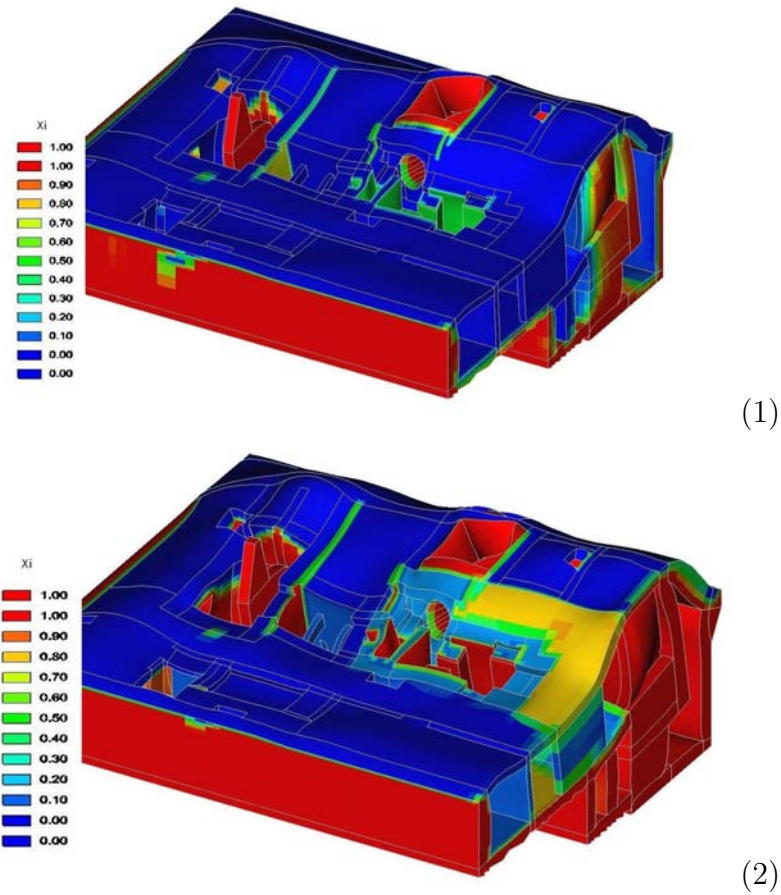


Figure 16: Deformed structure at $t_p = 40$ years (1) and at $t_f = 100$ years (2); colours represent the AAR-extent, from 0. (dark blue) to 1. (dark red).

5 $\mu\text{m}/\text{m}$) shall be remembered here. This table proves the relevance of the numerical simulation: the expansion model has been fitted on global structural measures (upper slab vertical displacements); then it gives fair agreement with independent monitoring of local behaviour.

5.2 Application to re-assessment

The application of the above-presented modeling is, at this time, a work in progress. To answer structure owner concerns, different points on the upper slab will be considered (anchorage of different sensitive equipments) and their displacements will be predicted. The obtained results will then be used to evaluate the future serviceability of the plant. For instance, as shown in Figure 18, one shall check whether group axis can be adapted to future anchorage vertical displacements twice larger than present raise.

The modeling will also be used to assess stresses induced in the structure by restrained swelling. For instance, Figure 19 describes compressive stress at time $t_p = 40$ years: the embedment of the lower part of the structure in the rock pit induces compressions, whereas

Table 3: Comparison between computed and measured strain rates (in μ strains per year) for distancemeter locations 1.2 and 1.6

Distancemeter	Measured strain rate	Model strain rate
DH 1.2	+ 6.01	+ 9.21
DV 1.2	+ 16.07	+ 15.80
DH 1.6	- 0.65	+ 5.47
DV 1.6	+ 29.51	+ 29.91

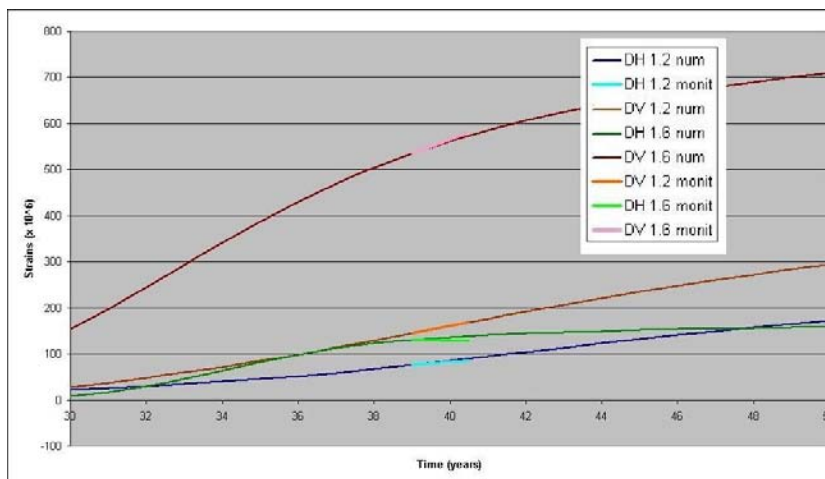


Figure 17: Computed strains for distancemeters DH 1.2, DV 1.2, DH 1.6 and DV 1.6; the light strokes represent the strain-rates measured in the structure

upper part is free to move.

It shall be noted that the stresses presented up to now are only generated by chemical expansion; they do not correspond to real stress-state, which will also be computed by introducing mechanical loads, in order to assess the real stress-state and, consequently, the structural reliability of the plant. This real stress-state will also be used to identify tensioned zones (at present time or in the future) in order to help designing structure repairs or reinforcements.

6 CONCLUSION

A global case-study was presented, concerning a real structure submitted to AAR-induced strains. Both complexity of structural behaviour and heterogeneous moisture field required the use of adapted numerical modeling: the model has to be easy to fit on the base of macroscopic laboratory tests and field measurements, but it must be rich enough to take into account coupling between moisture, temperature and reaction development.

Through this case-study, different phases of model fitting were described. It required an extensive monitoring of the structure, a large sampling of material used for laboratory tests

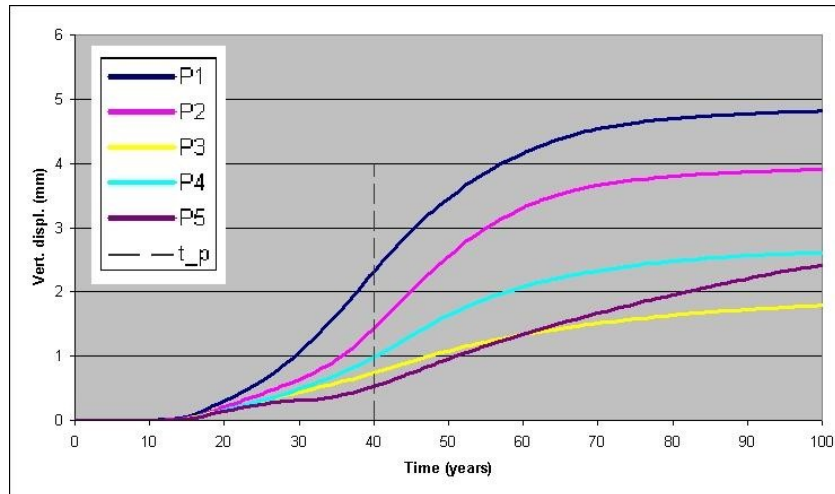


Figure 18: Predicted vertical displacement for points $P_1 \dots P_5$; dashed line represents present time t_p

and series of numerical computations to refine constitutive laws with an inverse problem philosophy. The results obtained with this global method (Godart et al. 2004) emphasize its relevance for re-assessment of AAR-affected structures: the fitting of the model on the sole base of global structural response gave fair results when compared to independent local structural monitoring.

This case-study intends to underline the strong interest of this method to answer practical problems of structure management: in the case of a hydro-power plant, modeling allows to correctly inform structure owner about stresses generated by the reaction in the structure as well as future disturbance in the equipments due to anchorage displacements, hence the loss of serviceability of the facility. Numerical modeling plays a large role as a long-term managing tool.

The work briefly described in these pages will continue with the study of stress field in the structure as well as the assessment of possible treatment techniques. In this goal, the constitutive model will be improved with latest results in chemo-mechanical modeling (Baghdadi et al. 2007).

Acknowledgements: The authors are pleased to thank Patricia Roure (Itech company) for her help in designing and using the numerical model.



Figure 19: Contour-plot for compressive stress generated by restrained swelling at present time - red represents low compressions, green means higher stress state

References

- Baghdadi, N., Toutlemonde, F., and Seignol, J.-F. (2007). Modélisation de l'effet des contraintes sur l'anisotropie de l'expansion dans les bétons atteints de réactions de gonflement interne. In AUGC (Ed.), *XXVèmes rencontres universitaires de génie civil*, Bordeaux.
- Charlwood, R. and Sans, J. B. (Eds.) (2007). *Chemical Expansion of Concrete in Dams & Hydro-Electric Projects*, Granada, Spain. Icold Committee on Concrete Dams, Spanish Committee on Concrete for Dams, International Journal on Hydropower and Dams. <http://dam-research.org/Granada-2007>.
- Fasseu, P. (1997). Alkali-réaction du béton - essai d'expansion résiduelle sur béton durci. Projet de méthode d'essai des LPC 44, Laboratoire central des ponts et chaussées, Paris.
- Godart, B., Mahut, B., Fasseu, P., and Michel, M. (2004). The guide for aiding to the management of structures damaged by concrete expansion in France. In M. Tang and M. Deng (Eds.), *12th Int. Conf. on Alkali-Aggregate Reaction in Concrete*, Beijing, pp. 1219–1228. International Academic Publishers, World Publishing Corporation.
- Humbert, P., Dubouchet, A., Fezans, G., and Remaud, D. (2005). CESAR-LCPC, un progiciel de calcul dédié au génie civil. *Bulletin des laboratoires des ponts et chaussées 256–257*, 7–37.
- Larive, C., Laplaud, A., and Coussy, O. (2000). The role of water in alkali-silica reaction. In *11th Int. Conf. on Alkali-Aggregate Reaction in Concrete*, Quebec, pp. 61–69.
- Li, K. and Capra, B. (2004). How to assess an ASR-affected concrete structure: from a consulting point of view. In M. Tang and M. Deng (Eds.), *12th Int. Conf. on Alkali-Aggregate Reaction in Concrete*, Beijing, pp. 933–938. International Academic Publishers, World Publishing Corporation.

- Li, K. and Coussy, O. (2002a). Concrete ASR degradation: from material modelling to structure assessment. *Concrete Science and Engineering 4*, 35–46.
- Li, K. and Coussy, O. (2002b). Numerical assessment of ASR-affected durability of concrete structures. In H. Mang, F. Rammerstorfer, and J. Eberhardsteiner (Eds.), *Proc. of the 5th World Congress on Computational Mech.*, Vienna.
- Li, K., Ulm, F.-J., and Coussy, O. (2001). Durability assessment of ASR-induced structural concrete degradation by a consistent model-based diagnosis-prognosis methodology. In Massachusetts Institute of Technology (Ed.), *Creep, Shrinkage and Durability Mech. Concrete and Other Quasi-brittle Materials*, Boston, USA, pp. 499–504.
- Li, K., Ulm, F.-J., Coussy, O., Larive, C., and Fan, L. (2000). Chemoelastic modelling of alkali-silica reaction in concrete. In *11th Int. Conf. on Alkali-Aggregate Reaction in Concrete*, Quebec, pp. 989–998.
- Multon, S. and Toutlemonde, F. (2006). Effect of applied stress on alkali-silica reaction-induced expansion. *Cement and Concrete Research 36*, 912–920.
- Seignol, J.-F., Ngo, T.-T., and Toutlemonde, F. (2006). Modelling of the coupling between moisture and alkali-silica reaction in concrete. In Meschke, de Borst, Mang, and Bićanić (Eds.), *Computational Modelling of Concrete Structures*, Mayrhofen.
- Ulm, F.-J., Coussy, O., Li, K., and Larive, C. (2000). Thermo-chemo-mechanics of ASR expansion in concrete structures. *J. Eng. Mech.* 126(3), 233–242.